Quantum Statistical Study of O + O_2 Isotopic Exchange Reactions: Cross Sections and Rate Constants†

Shi Ying Lin and Hua Guo*

Department of Chemistry, University of New Mexico, Albuquerque, New Mexico 87131

Received: October 3, 2005; In Final Form: November 1, 2005

Using a wave packet based statistical model, we compute cross sections and thermal rate constants for various isotopic variants of the O + O_2 exchange reaction on a recently modified ab initio potential energy surface. The calculation predicts a highly excited rotational distribution and relatively cold vibrational distribution for the diatomic product. A small but important threshold effect was identified for the $^{16}O + {}^{18}O_2$ reaction, which is suggested to contribute to the experimentally observed negative temperature dependence of the rate ratio, $k(^{18}O + {}^{16}O_2)/k(^{16}O + {}^{18}O_2)$. Despite reasonable agreement with quasiclassical trajectory results, however, the calculated thermal rate constants are smaller than experimental measurements by a factor from 2 to 5. The experimentally observed negative temperature dependence of the rate constants is not reproduced. Possible reasons for the theory−experiment discrepancies are discussed.

I. Introduction

Ozone is one of the most extensively studied small polyatomic molecules due to its crucial importance in atmospheric chemistry. Despite vast efforts, however, our understanding of this molecular system is still far from complete. The recent surge of activities stems largely from the discovery of unexpected isotope effects in the formation of ozone in the earth atmosphere and in laboratories.[1−3] The rate for third-body assisted recombination of O_3 from O and O_2 was found to depend on the isotope combination of the three oxygen atoms involved. It is now experimentally established that these so-called "mass-independent" isotope effects have a quantum mechanical origin, evidenced by a linear correlation between the recombination rate constants and zero-point energy differences of various O_2 isotopes.[4] These observations have stimulated many theoretical investigations of the potential energy surface (PES) of ozone,[5−10] as well as the nuclear dynamics.[11−27]

In addition to the formation of ozone, the collision of O and O_2 may lead to isotopic exchange reactions:

$$O(^3P) + O'O''(\tilde{X}^3\Sigma_g^-) \rightarrow OO'(\tilde{X}^3\Sigma_g^-) + O''(^3P)$$

which are the focus of this theoretical study. Although interests on the exchange reactions started a long time ago,[28−30] reliable experimental measurements have only been reported recently. Anderson et al.[31] published the first trustworthy experimental study on the exchange reaction rates at room temperature, which showed significant isotope effects. As in the ozone recombination reaction, the origin of the isotope effects in the exchange reaction is also believed to be quantum mechanical. Later, Wiegell et al.[32] measured the rate constant at different temperatures with mixed isotopes, which showed a negative temperature dependence. Very recently, Fleurat-Lessard et al.[18] published detailed experimental and theoretical investigations of various isotopic variants of the exchange reaction at multiple temperatures. Their experimental results are in general consistent with the earlier data of Anderson et al.[31] and Wiegell et al.[32] One of the quantities measured by the most recent experimental work[18] is the ratio of two rate constants ($R = k(^{18}O + {}^{16}O_2)/k(^{16}O + {}^{18}O_2)$), which itself has a negative temperature dependence.

Theoretical investigations of the exchange reaction also have a long history,[15,18,19,23,24,33−38] but the lack of an accurate PES and difficulties in quantum mechanical characterization of the reaction dynamics limited the reliability of their conclusions. Recently, the situation has improved dramatically for the description of the ground-state ozone PES. For example, Siebert, Schinke, and Bittererova[6] (SSB) constructed a new global PES based on high level ab initio (MRCI/cc-pVQZ) calculations. The SSB PES is very accurate in the ozone well, as evidenced by the excellent agreement of the calculated ozone vibrational spectrum with experimental results up to a high energy (85% of dissociation energy).[7] Because it possesses a qualitatively incorrect barrier in the dissociation channels, however, the SSB PES is not well suited for dynamical studies of O + O_2 collisions. Higher level ab initio calculations[9,10,19] indicated that this barrier should be below the dissociation limit, making it a "reef-like" structure with an asymptotic van der Waals well. The SSB PES was thus modified empirically by Babikov et al.[23] to produce the correct asymptotic potential topology, and this version of the PES was used in this work.

Because the isotope effects are likely originated from the zero-point energy differences of isotopically different O_2, the dynamic model must include the proper treatment of the quantum property. The rigorous inclusion of zero-point energies in a classical model is difficult (see ref 18), so a quantum treatment is preferred. Quantum characterization of the exchange reaction has, however, met stiff resistance due to the heavy particle nature of the system and the involvement of a deep potential well, which supports long-lived resonances above the reaction threshold. The first converged exact time-independent quantum reactive scattering studies of the exchange reaction was restricted to $J = 0$.[19,23,24] These investigations discovered that the reaction is dominated near the reaction threshold by extremely long-lived resonances, which require a very large basis to achieve

† Part of the special issue "John C. Light Festschrift".

* Corresponding author. E-mail: hguo@unm.edu. Fax: 505 2772609.

10.1021/jp0556299 CCC: $33.50
Published on Web 12/06/2005

convergence. An impressive quantum wave packet study of the total reaction probabilities for the hypothetical $^{16}O + {}^{16}O_2$ ($v_i = 0, j_i = 0$) exchange reaction was later reported for J up to 25.[15] Strong oscillations were also found, which can be attributed to the long-lived resonances. As a result, the propagation time was exceedingly long. The coupled-state (CS) approximation[39,40] was found to introduce significant errors, consistent with earlier findings for other complex-forming reactions.[41,42] In addition, the wave packet work was for the $j_i = 0$ state of $^{16}O_2$, which is forbidden by nuclear spin statistics. No state-to-state scattering attribute has been reported. Even systematic classical studies of final state distributions are to our best knowledge nonexistent in the literature.

As discussed in recent literature,[43−49] the long lifetime of collisional resonances in complex-forming reactions often allows a statistical characterization, because the dynamical memory is scrambled by the long-lived reaction intermediate. The $O + O_2$ exchange reaction, which is dominated by the long-lived ozone intermediate and nearly thermoneutral, seems to suggest itself as an ideal candidate for such a treatment. (We note, however, that nonstatistical behaviors have been noted by a recent classical study of ozone decomposition.[18]) In the statistical model, state-to-state reaction probabilities are obtained from capture probabilities, which can be readily computed quantum mechanically in each arrangement channel. Provided that the asymptotic capture dynamics is treated accurately using a realistic PES, the agreement with exact quantum results has been demonstrated for a number of complex-forming atom−diatom reactions to be quite accurate. Encouraged by the success of these quantum statistical studies, we investigated in this work the following three isotope variants of the exchange reaction using a wave packet based statistical model[46]

$$^{16}O + {}^{18}O_2 \rightarrow {}^{16}O^{18}O + {}^{18}O \quad \text{(R1)}$$

$$^{18}O + {}^{16}O_2 \rightarrow {}^{18}O^{16}O + {}^{16}O \quad \text{(R2)}$$

$$^{16}O + {}^{16}O_2 \rightarrow {}^{16}O^{16}O + {}^{16}O \quad \text{(R3)}$$

The integral cross sections as well as thermal rate constants were calculated for R1 and R2. For R3, only initial state-specified total cross sections and rate constants for two selected initial states ($j_i = 1, 9$) were computed. These results were compared with available experimental data and previous quasiclassical trajectory results. This paper is organized as follows. In the next section (Sec. II), the theoretical method is briefly outlined. In section III, numerical implementations and the calculated results are presented and discussed. Finally in section IV, conclusions are made.

II. Theory

The ground-state PES for $O_3(X^1A')$ features three symmetry equivalent potential minima corresponding to the C_{2v} ozone molecule. These minima can be accessed from the $O + O_2$ asymptotes via barrierless pathways and the dissociation energy is slightly more than 1.0 eV. The ozone wells support many bound and resonance states, and some of them participate in the exchange reaction. The lifetimes of these resonance states have been reported to be on the ns scale, using both quantum mechanical[23,24] and classical methods.[16] Their dominance in the reaction presents a huge challenge for exact quantum characterization of the exchange reaction. Paradoxically, these characteristics offer an opportunity to understand the reaction from a statistical perspective.

The basic premise of the statistical approach[50−53] is that the reaction complex lives sufficiently long so that dynamic information is completely scrambled. As a result, the state-to-state reaction probability, $p_{f\leftarrow i}(E)$, can be expressed as a product of the capture probability ($p^{(c)}$) in the reactant (i) channel and the fraction of population decaying into the product (f) channel (where i or f collectively denotes the particular quantum states in the reactant or product channel):

$$p_{f\leftarrow i}(E) = p_i^{(c)}(E)\frac{p_f^{(c)}(E)}{\sum_l p_l^{(c)}(E)} \quad (1)$$

The summation in the denominator of eq 1 runs over all the open channels at energy E. Conserved indices, such as the total angular momentum (J) and parity (I) are suppressed.

In the original phase space theory (PST) proposed by Light and Pechukas,[50−52] the capture probabilities were obtained using a classical model. No realistic potential is needed, and dynamical effects are ignored. Recently, PST was improved by Manolopoulos and co-workers,[43−45] who computed explicitly the capture probabilities using a time-independent quantum method. Semiquantitatively accurate integral and differential cross sections were obtained for several insertion reactions dominated by long-lived resonances, with only a fraction of the costs. In contrast to direct quantum calculations of reaction probabilities, the capture probabilities are much more efficiently obtainable because of two major reasons. First, only one arrangement channel needs be considered in each calculation, so that coordinate transformation is unnecessary. Second, long-time propagation is avoided, because the capture process is fast. In addition, only potentials in the asymptotic regions are needed. An important feature of this improved version of the statistical model is that quantum effects in the capture process, including tunneling and zero-point energy, are rigorously included.

The capture probabilities can also be calculated using a wave packet method.[46] Because the energy global approach yields reaction probabilities at all energies with a single propagation, it is ideally suited for calculating the rate constant which requires energy dependency of the reaction probabilities. In addition, wave packet approaches typically scale better than time-independent methods. In this work, we employed the wave packet implementation of the statistical model with the Chebyshev propagator.[54] The capture probabilities were computed using a flux approach. The readers are referred to the original work[46] for details.

On a cautionary note, it should be stressed that the validity of the statistical model is based on the statistical nature of a reaction, which can only be established by comparing with experimental or exact quantum mechanical data. However, the results reported here can always be considered as a limiting case to measure how statistical the exchange reactions really are.

With the state-to-state reaction probabilities for various J, initial state-specified total integral cross sections (ICSs or $\sigma_i(E_c)$) can be calculated by summing over all partial waves and final states. The corresponding rate constant can then be obtained by a Boltzmann average of $\sigma_i(E_c)$ over the collision energy E_c:

$$k_i = Q_{el}^{-1}\sqrt{\frac{8}{\pi\mu(k_B T)^3}}\int_0^\infty \sigma_i(E_c)\exp(-E_c/k_B T)E_c\, dE_c \quad (2)$$

where μ, k_B, and T are the translational reduced mass, Boltzmann constant, and temperature, respectively. Q_{el} is the electronic partition function for the exchange reaction, which is given by[38]

$$Q_{el} = 3[5 + 3\exp(-227.6/T) + \exp(-325.9/T)] \quad (3)$$

where T is in the unit of Kelvin. The thermal rate constant can finally be obtained by averaging the initial state-specified rate constants for all thermally accessible initial states weighted by the Boltzmann factor. The statistical treatment of the electronic degeneracy in the asymptote is reasonable as suggested by recent work of Tashiro and Schinke.[20]

With an additional random phase approximation, the differential cross section (DCS) can also be calculated.[44] We have obtained the DCS for these reactions, but the results are not shown because the difference between the R1 and R2 reactions is not significant and all of them show typically forward−backward symmetry, which is mandated by the random phase approximation.

III. Results and Discussion

A. Numerical Aspects. The appropriate Jacobi coordinates, R (O−OO distance), r (O−O distance) and γ (Jacobi angle), were used in each arrangement channel. The Hamiltonian was discretized in a mixed discrete variable/finite basis representation (DVR/FBR). For R, an equidistant grid was defined and the translational kinetic energy operator was evaluated using fast sine Fourier transformation.[55] For r, the corresponding rovibrational Hamiltonian was discretized with potential optimized DVR (PODVR).[56,57] For the angular dimension, both the FBR (associate Legendre functions) and DVR (Gauss-Legendre quadrature points)[58] were used interchangeably. The rotational kinetic energy operators were calculated in the FBR, whereas the potential energy operator is the DVR. The modified SSB PES[23] was employed. The numerical parameters were determined through extensive convergence tests and their values are summarized below.

As the masses of different isotopic variants are slightly different, the parameters required for convergence can vary. We chose parameters that are somewhat oversized so that the same parameter set applies to all arrangement channels. An exception is the angular basis size which is different in the $^{16}O + {}^{16}O_2$, $^{18}O + {}^{16}O_2$, $^{16}O + {}^{18}O_2$ arrangement channels and in the $^{16}O + {}^{16}O^{18}O$,$^{18}O + {}^{16}O^{18}O$ arrangement channels. For the former, the permutation symmetry can be applied, and as a result, their angular basis is smaller than the latter by a factor of 2. For the angular dimension, 30 Gauss−Legendre quadrature points between $\gamma = 90°$ and 180°, and $j = 1, 3, ..., 59$ were chosen for those arrangement channels involving homonuclear diatoms, whereas 60 Gauss−Legendre quadrature points between $\gamma = 0°$ and 180°, and $j = 0, 1, ..., 59$ were chosen for those channels involving heteronuclear diatoms. For R, 255 grid points were taken between 0.1 and 17.0 a_0 and 2 PODVR points were used for r.

Damping functions with the exponential ($e^{-\alpha(R-R_{d,c})^2}$) form were applied in both the asymptotic region starting from $R_d = 13.0\ a_0$ with absorption coefficient of $\alpha = 0.001\ a_0^{-2}$ and the capture region starting from $R_c = 3.8\ a_0$ with absorption coefficient of $0.1\ a_0^{-2}$. The flux entering into the well was calculated at $R_f = 3.9\ a_0$. An initial wave packet with a standard Gaussian form was launched at $R_i = 10.0\ a_0$ with width of $0.2\ a_0^{-2}$ and an average kinetic energy of 0.15 eV. The wave packet was propagated up to 10 thousand Chebyshev steps. The CS approximation was employed in the capture probability calculations. The calculations were repeated for all possible J values up to $J_{max} = 100$. We focused our attention to the $^{18}O + {}^{16}O_2$ and $^{16}O + {}^{18}O_2$ reactions, whose cross sections were calculated up to $j_i = 23$ to obtain thermal rate constants. For the $^{16}O + {}^{16}O_2$ reaction, we only reported results for $j_i = 1$ and 9.

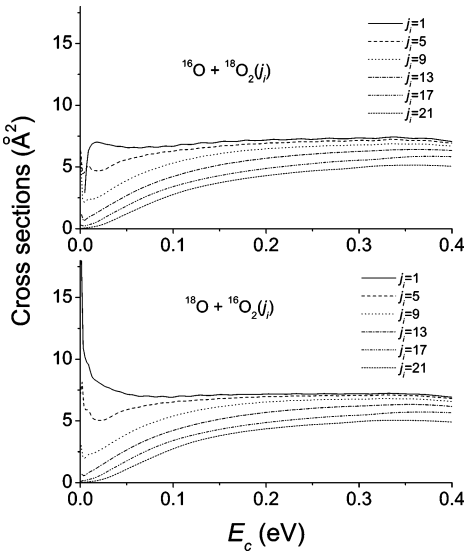

Figure 1. Energy dependence of initial state ($v_i = 0, j_i$) specified total cross sections for R1 (upper panel) and R2 (lower panel) reactions.

B. Total Integral Cross Sections and Rate Constants. We first examine the initial state dependence of the total integral cross section. In Figure 1, the integral reaction cross sections of the $^{16}O + {}^{18}O_2$ and $^{18}O + {}^{16}O_2$ reactions are plotted as a function of the collision energy (E_c) for a number of initial rotational states of the diatomic reactant. Note that all even rotational states of the reactant O_2 are unpopulated because of the nuclear spin statistics. For both reactions, the cross section depends sensitively on the initial rotational state. Such a strong dependence on the initial rotational excitation has been noted before in quasiclassical trajectory studies of the exchange reaction on a number of PESs.[18,19,33,34] The reduction of reactivity by exciting the O_2 rotational state can be attributed to the narrow bottleneck of the reaction,[6,7,19] i.e., the transition state in the entrance channel, which renders a rotating molecule more difficult to enter the reaction region. Similar dependence of the rate constant on the initial rotational state can also be expected. Indeed, the initial state-specified rate constant (not shown) decreased sharply with the increase of initial rotational excitation.

As j_i increases, the cross section increasingly exhibits a reaction threshold. This is understandable because of the escalating dominance of the centrifugal barrier in the entrance channel. At large collision energies significantly above the centrifugal barrier, however, the cross section typically levels off. Unlike the quasiclassical trajectory results in which the j_i dependence diminishes at large E_c,[18,19] the statistical cross sections still show significantly differences at large collision energies. The energy dependence of the cross section ultimately determines the temperature dependence of the thermal rate constant. As discussed in earlier work on this reaction,[19] the energy dependence is in turn related to the topology of the PES in the transition state region.

The cross sections computed using the statistical model appear to be significantly larger than their quasiclassical trajectory counterparts, as reported by Schinke and co-workers.[18] A direct comparison was not possible because of only results for even rotational states were reported in the quasiclassical trajectory

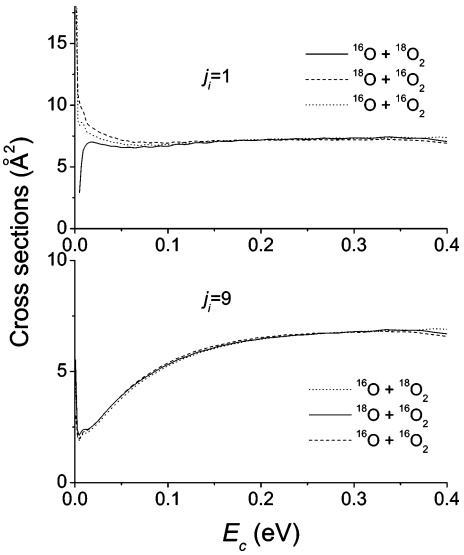

Figure 2. Comparison of initial state specified total cross sections between three different isotopic reactions R1, R2, and R3, for two selected initial states $j_i = 1$ (upper panel) and $j_i = 9$ (lower panel).

study and the PES is somewhat different. Nonetheless, the larger statistical cross sections could be due to the underestimation of inelastic scattering back to the entrance channel, namely overestimation of the capture probabilities.

Interestingly, the behavior of the cross section is quite different for the R1 and R2 reactions involving the lowest rotational state of O_2. In Figure 2, we compare the cross sections for the three isotopic reactions for $j_i = 1$ and 9. For both the $^{18}O + {}^{16}O_2(j_i = 1)$ and $^{16}O + {}^{16}O_2(j_i = 1)$ reactions, the cross sections decrease sharply with E_c at low collision energies, indicating a (nearly) barrierless reaction pathway. On the other hand, the cross section of the $^{16}O + {}^{18}O_2(j_i = 1)$ reaction is small at low collision energies and increases with E_c. For a higher rotational state ($j_i = 9$), however, this difference disappears. The decreasing cross section at very low collision energies is due to the kinematic factor ($1/k_i^2$) in the cross-section. A careful examination of the reaction exothermicity explains the isotopic effect. The threshold effect observed for the $^{16}O + {}^{18}O_2(j_i = 1)$ reaction is due to the small endothermicity of the R1 reaction ($\sim$20 cm^{-1}), counting the zero-point energy difference between the reactant and product. On the other hand, R2 is exothermic by 25 cm^{-1} and R3 is thermoneutral. In other words, the threshold effect in R1 is essentially due to the endothermic barrier, which in turn stems from the zero-point energy difference between the reactant and product. At large collision energies, understandably, the isotopic difference is very small as the contribution of the threshold effect diminishes.

The threshold effect observed in the cross section is also reflected in the rate constant. In Figure 3, the initial state-specified ($j_i = 1$ and $j_i = 9$) rate constants are compared between three different isotopic reactions. As expected, for $j_i = 1$, the rate constant for the $^{16}O + {}^{18}O_2$ reaction is substantially smaller than those for the other two, especially at low temperatures. For $j_i = 9$, the difference between them becomes negligible.

In Figure 4, the temperature dependence of thermal rate constants of two isotopic reactions, R1 and R2, is depicted and compared with available experimental[18,31,32] and previous theoretical data.[18,19] As the figure shows, the agreement is not quantitative. Our statistical model predicts significantly smaller rates than the experimental data. The difference is as large as an order of magnitude at very low temperatures and a factor of 2 $\sim$ 5 at higher temperatures. At 300 K for example, the

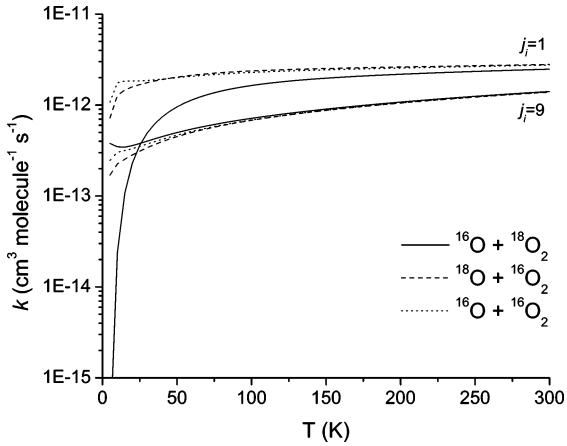

Figure 3. Comparisons of initial state specified rate constants between three different isotopic reactions R1, R2, and R3, for two selected initial states $j_i = 1$ and $j_i = 9$.

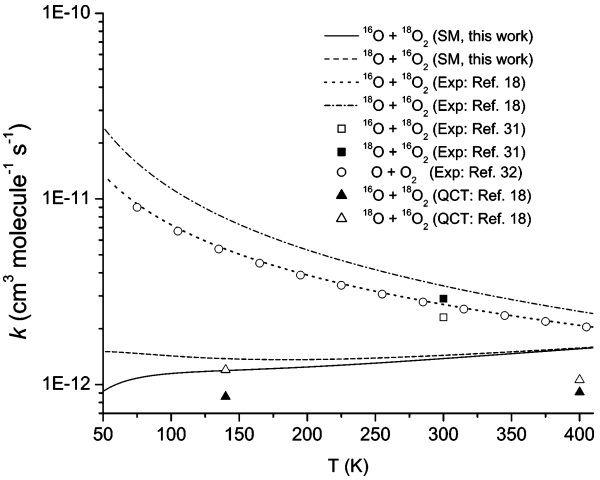

Figure 4. Temperature dependence of thermal rate constants for reactions R1 and R2, calculated by the quantum statistical model, by a quasiclassical trajectory method,[18] and their comparison with experimental results.[18,31,32]

statistical rate constants for reactions R1 and R2 are 1.38×10^{-12} and 1.44×10^{-12} cm^3 molecule^{-1} s^{-1}, respectively, which can be compared with the latest experimental values of $(2.7 \pm 0.4) \times 10^{-12}$ and $(3.4 \pm 0.6) \times 10^{-12}$ cm^3 molecule^{-1} s^{-1}.[18] In addition, our results show that the thermal rate constants for the two reactions are almost temperature independent, whereas experimental investigations[18,32] reported clear negative temperature dependence.

Interestingly, our quantum statistical model shares many common features with the quasiclassical trajectory results reported by Fleurat-Lessard et al.,[19] who used a similar version of the SSB PES. Both underestimate the rate constants and failed to reproduce the experimentally observed negative temperature dependence. This quantum-classical similarity essentially rules out the possibility that the neglect of quantum effects in the quasiclassical trajectory calculations is responsible for the failure in reproducing the experimental findings. Other possible causes for the disagreement will be discussed later.

One key quantity that has been measured experimentally and computed theoretically is the ratio of the rate constants for reactions R1 and R2: $R = k(^{18}O + {}^{16}O_2)/k(^{16}O + {}^{18}O_2)$.[18] Apart from the higher precision achievable in the experimental measurement, this quantity has also the advantage that potential errors introduced in the statistical treatment of the nonadiabatic effects in the entrance channel are likely equalized.[18] In Figure

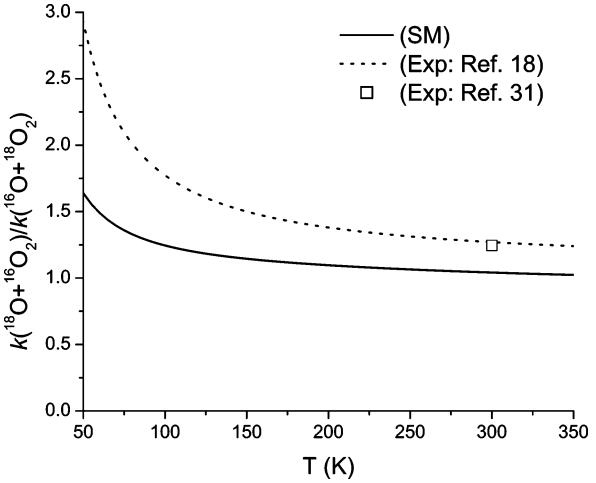

Figure 5. Temperature dependence of the ratio of thermal rate constants of R2 and R1 calculated by quantum statistical model and its comparison with experimental results.[18]

5, this ratio is plotted as a function of temperature and compared with the experimental data. The calculated ratio has the same trend as the experimental data; i.e., both ratios show negative temperature dependence and are larger than unity. Quantitatively, however, our result is somewhat smaller than the experimental counterpart. At 300 K, our ratio is 1.04 whereas the experimental value is 1.27 ± 0.04. The quasiclassical trajectory calculations,[19] on the other hand, reported a room-temperature ratio of between 1.0 and 1.3, depending on how the zero-point energy is treated.[18] The discrepancy between the theory and experiment is still not elucidated.

The negative temperature dependence of the rate ratio can be attributed, at least in part, to the threshold effect discussed in Figure 2. Due to its endothermicity, reaction R1 has a small reaction threshold for the lowest rotational state $j_i = 1$, whereas reaction R2 has none. This small disparity due to zero-point energy difference is shown in Figure 3 to result in a substantial difference in the initial state-specified rate constants at low temperatures. Because the thermal rate constant is dominated in this temperature region by the lowest reactant state and small collision energies, the small threshold isotope effect is amplified in *R*. As temperature increases, the role of the threshold effect diminishes and *R* approaches unity.

Schinke and co-workers[19] have reported results obtained from the statistical adiabatic channel model (SACM).[59] Interestingly, the SACM results showed significantly larger deviations from the quasiclassical trajectory data than those obtained from the statistical model used in this work. Because tunneling is expected to be negligible in this heavy system, the major difference between the current statistical model and SACM is that the latter assumes adiabaticity for the internal states of the reactants. As a result, the success of our statistical model is presumably due to the quantum dynamical treatment of the capture processes. Indeed, significant rotational nonadiabaticity was observed in the quasiclassical trajectory studies of these exchange reactions.[19]

C. Product State Distributions. So far, there has been no experimental information on either the final state or angular distribution of the product in the exchange reaction. Theoretical predictions are also scarce. In this work, we report ro-vibrational state distributions using the statistical model, hoping to stimulate experimental exploration of the state-to-state aspects of the exchange reaction. In Figure 6, the product vibrational state resolved integral cross sections of two isotopic exchange

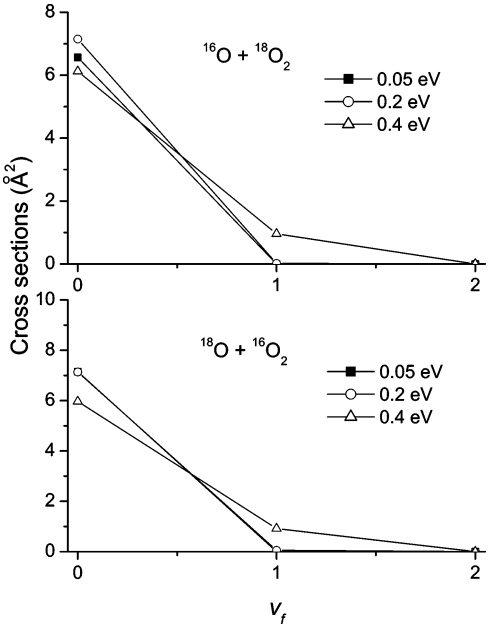

Figure 6. Product vibrational state distributions (for initial state of $v_i = 0, j_i = 1$) for the R1 (upper panel) and R2 reactions (lower panel) at three selected collision energies.

reactions (R1 and R2) are displayed for several selected collision energies. The diatomic reactant was in its lowest possible state ($v_i = 0$, $j_i = 1$), but rotational excitation in the incoming diatom does not significantly change the picture. As the figure shows, in both reactions, the products are predominantly generated in the ground vibrational state, with increasing populations in excited vibrational states at higher energies. Such a monotonically decaying vibrational state distribution is a fingerprint of complex-forming reactions.

In Figure 7, rotational state resolved integral cross sections in the v_f=0 manifold for two isotopic exchange reactions (R1 and R2) are depicted for two initial rotational states $j_i = 1$ and $j_i = 9$. In contrast to the vibrational state distributions, the rotational state distributions are highly excited. With the increase of collision energy, the distributions broaden and the quantum number corresponding to the maximum population shifts toward higher rotational states. The high rotational excitation in the products has also been seen in quasiclassical trajectory calculations.[19] The highly excited product rotational state distribution is another signature of complex-forming reactions. The difference between the two isotopic variants is not significant.

IV. Conclusions

In this work, we presented a quantum statistical study of the O + O_2 exchange reaction with various isotopic variants. The statistical treatment appears to be reasonable judging by the long lifetime of the ozone intermediate which dominates the exchange reaction at low energies, although its validity has to be established ultimately by comparing with exact quantum mechanical calculations. This work differs from previous theoretical studies in several important aspects. First, it treats the complex-forming and complex-decomposition dynamics quantum mechanically on the most accurate ab initio PES to date. As a result, quantum effects such as the zero-point energy and ro-vibrational nonadiabaticity are all included in the model. Second, it includes all the partial waves so that the calculated attributes, such as cross sections and rate constants, can be directly compared with experimental measurements.

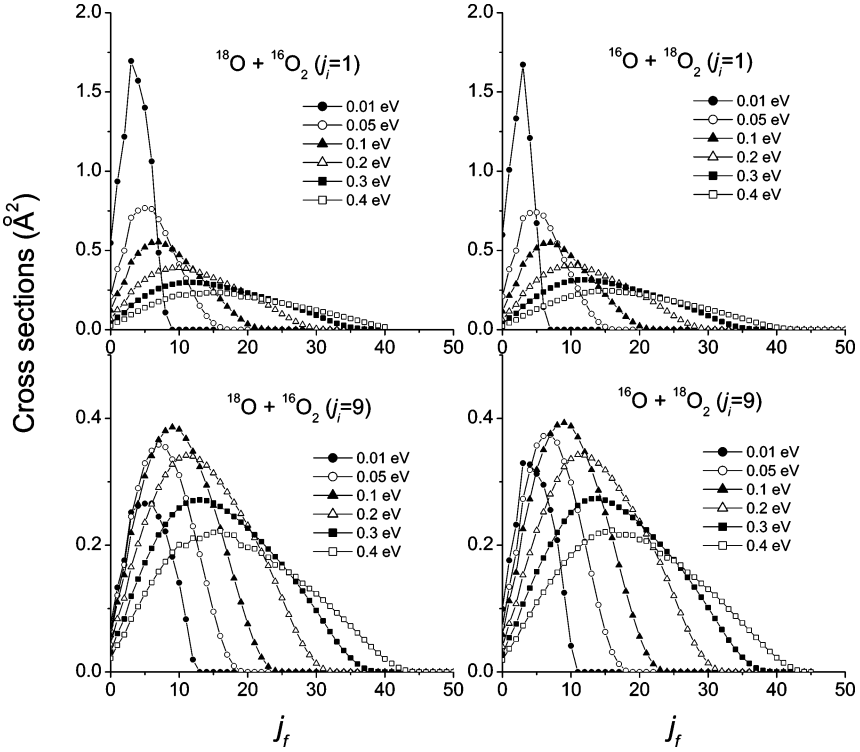

Figure 7. Product rotational state distributions in the $v_f = 0$ manifold (for initial states of $v_i = 0, j_i = 1$ and $v_i = 0, j_i = 9$) for the R1 and R2 reactions at six selected collision energies.

To this end, state resolved integral cross sections and thermal rate constants for various isotopic variants of the title reaction have been calculated. In all reactions, the integral cross section decreases with increasing excitation in the rotational state of the reactant, due apparently to the narrowness of the transition state in the angular coordinate. Quantitatively, the calculated thermal rate constants were smaller than the experimental measurements by a factor of 2−5. The isotopic effects observed in our theoretical calculations were not as pronounced as in experimental observations. The statistical model predicts that the product of the exchange reactions is vibrationally cold and rotationally hot, and the angular distributions were found to be forward−backward symmetric.

The behavior of the exchange reaction can be quite different for different isotope combinations at very low collision energies. We showed that from the lowest reactant rotational state ($j_i = 1$), the $^{16}O + {}^{18}O_2$ reaction exhibits a reaction threshold, which signifies a barrier, whereas other exchange reactions show no such threshold. The observed threshold is attributed to the small ($\sim$20 cm^{-1}) endothermicity of the reaction R1 stemming from the zero-point energy difference between the reactant and product. Such a difference near the reaction threshold is amplified in the low-temperature rate constant but becomes less pronounced at higher temperatures when rate constants for higher j_i states and higher collision energies bury the isotope effect. This observation provides a rationalization of the observed monotonic decay of the rate ratio ($R = k(\mathrm{R1})/k(\mathrm{R2})$) as a function of temperature.

Our quantum statistical model yielded results that are qualitatively consistent with recent quasiclassical trajectory studies, which were also performed on similar PESs. Both showed significant deviations from the experimental rates and their temperature dependence. The consistency between quantum and classical rate constants all but eliminated the possibility that some quantum effects are responsible for the theory-experiment discrepancy. There are several other possible sources in the theoretical treatment of the dynamics that may cause errors. One is the neglect of nonadiabatic effects in the asymptotic channels. There are 27 degenerate electronic states in the $O + O_2$ asymptote, and most of them are repulsive. Tashiro and Schinke[20] have shown that the statistical treatment of the spin−orbit components is a good approximation. However, other nonadiabatic couplings have not been examined. We note in passing that the statistical model works well in other reactions involving electronically near-degenerate asymptotic states.[45] Another possible source of error is the accuracy of the PES. Previous theoretical studies have demonstrated that detailed topology near the transition state has a surprisingly large effect on the rate constant and its temperature dependence. Despite much work in this aspect, it is still too early to conclude on the accuracy of the PES.

Significant errors can of course be introduced through the statistical approach. Nonstatistical factors have been shown to be important in reproducing the experimental rate constant of ozone formation.[12,13] Fleurat-Lessard et al. have also shown explicitly with classical trajectories that the decomposition of ozone is not statistical, particularly at high energies.[18] For exchange reactions, the reasonably good agreement between statistical and quasiclassical rate constants seems to suggest that the nonstatistical factor may be small. However, rate constants are highly averaged quantities that might harbor substantial canceling errors in more detailed attributes such as state-resolved cross sections. Thus, it is important to compare our state-resolved scattering information with both exact quantum and quasiclassical results in the future. Experimental studies on these quantities, though difficult, will provide further assessment about the validity of the statistical model.

Acknowledgment. This work is dedicated to Prof. John C. Light, who has, among his many great contributions to chemical physics, pioneered the statistical treatment of complex-forming chemical reactions. Financial support from the Department of

Energy (DE-FG02-05ER15694) and the National Science Foundation (CHE-0348858) is gratefully acknowledged. We thank Prof. Reinhard Schinke for sending us the potential energy surface used in the calculation.

References and Notes

(1) Mauersberger, K. *Geophys. Res. Lett.* **1981**, *8*, 935.
(2) Thiemens, M. H.; Heidenreich, J. E., III. *Science* **1983**, *219*, 1073.
(3) Mauersberger, K.; Krankowsky, D.; Janssen, C.; Schinke, R. *Adv. At. Mol. Opt. Phys.* **2005**, *50*, 1.
(4) Janssen, C.; Guenther, J.; Krankowski, D.; Mauersberger, K. *Phys. Chem. Chem. Phys.* **1999**, *3*, 4718.
(5) Xie, D.; Guo, H.; Peterson, K. A. *J. Chem. Phys.* **2000**, *112*, 8378.
(6) Siebert, R.; Schinke, R.; Bittererova, M. *Phys. Chem. Chem. Phys.* **2001**, *3*, 1795.
(7) Siebert, R.; Fleurat-Lessard, P.; Schinke, R.; Bittererova, M.; Farantos, S. C. *J. Chem. Phys.* **2002**, *116*, 9749.
(8) Rosmus, P.; Palmieri, P.; Schinke, R. *J. Chem. Phys.* **2002**, *117*, 4871.
(9) Hernandez-Lamoneda, R.; Salazar, M. R.; Pack, R. T. *Chem. Phys. Lett.* **2002**, *355*, 478.
(10) Schinke, R.; Fleurat-Lessard, P. *J. Chem. Phys.* **2004**, *121*, 5789.
(11) Hathorn, B. C.; Marcus, R. A. *J. Chem. Phys.* **1999**, *111*, 4087.
(12) Gao, Y. Q.; Marcus, R. A. *Science* **2001**, *293*, 259.
(13) Gao, Y. Q.; Marcus, R. A. *J. Chem. Phys.* **2002**, *116*, 137.
(14) Charlo, D.; Clary, D. C. *J. Chem. Phys.* **2002**, *117*, 1660.
(15) Yeh, K.-L.; Xie, D.; Zhang, D. H.; Lee, S.-Y.; Schinke, R. *J. Phys. Chem.* **2003**, *A107*, 7215.
(16) Schinke, R.; Fleurat-Lessard, P.; Grebenshchikov, S. Y. *Phys. Chem. Chem. Phys.* **2003**, *5*, 1966.
(17) Grebenshchikov, S. Y.; Schinke, R.; Fleurat-Lessard, P.; Joyeux, M. *J. Chem. Phys.* **2003**, *119*, 6512.
(18) Fleurat-Lessard, P.; Grebenshchikov, S. Y.; Schinke, R.; Janssen, C.; Krankowsky, D. *J. Chem. Phys.* **2003**, *119*, 4700.
(19) Fleurat-Lessard, P.; Grebenshchikov, S. Y.; Siebert, R.; Schinke, R.; Halberstadt, N. *J. Chem. Phys.* **2003**, *118*, 610.
(20) Tashiro, M.; Schinke, R. *J. Chem. Phys.* **2003**, *119*, 10186.
(21) Ivanov, M. V.; Grebenshchikov, S. Y.; Schinke, R. *J. Chem. Phys.* **2004**, *120*, 10015.
(22) Schinke, R.; Fleurat-Lessard, P. *J. Chem. Phys.* **2005**, *122*, 094317.
(23) Babikov, D.; Kendrick, B. K.; Walker, R. B.; Pack, R. T.; Fleurat-Lesard, P.; Schinke, R. *J. Chem. Phys.* **2003**, *118*, 6298.
(24) Babikov, D.; Kendrick, B. K.; Walker, R. B.; Schinke, R.; Pack, R. T. *Chem. Phys. Lett.* **2003**, *372*, 686.
(25) Babikov, D.; Kendrick, B. K.; Walker, R. B.; Pack, R. T.; Fleurat-Lessard, P.; Schinke, R. *J. Chem.* Phys. **2003**, *119*, 2577.
(26) Lee, H.-S.; Light, J. C. *J. Chem. Phys.* **2004**, *120*, 5859.
(27) Xie, T.; Bowman, J. M. *Chem. Phys. Lett.* **2005**, *412*, 131.
(28) Herron, J. T.; Klein, F. S. *J. Chem. Phys.* **1964**, *40*, 2731.
(29) Brennen, W.; Niki, H. *J. Chem. Phys.* **1965**, *42*, 3725.
(30) Jaffe, S.; Klein, F. S. *J. Chem. Soc., Faraday Trans.* **1966**, *62*, 3135.
(31) Anderson, S. M.; Klein, F. S.; Kaufman, F. *J. Chem. Phys.* **1985**, *83*, 1648.
(32) Wiegell, M. R.; Larsen, N. W.; Pedersen, T.; Egsgaard, H. *Int. J. Chem. Kinet.* **1997**, *29*, 745.
(33) Stace, A. J.; Murrell, J. N. *J. Chem. Soc., Faraday Trans. 2* **1978**, *74*, 2182.
(34) Varandas, A. J. C.; Murrell, J. N. *Chem. Phys. Lett.* **1982**, *88*, 1.
(35) Varandas, A. J. C.; Pais, A. A. C. C. *Mol. Phys.* **1988**, *65*, 843.
(36) Gross, A.; Billing, G. D. *Chem. Phys.* **1993**, *173*, 393.
(37) Chajia, M.; Jacon, M. *J. Chem. Phys.* **1994**, *101*, 271.
(38) Gross, A.; Billing, G. D. *Chem. Phys.* **1997**, *217*, 1.
(39) Pack, R. T. *J. Chem. Phys.* **1974**, *60*, 633.
(40) McGuire, P.; Kouri, D. J. *J. Chem. Phys.* **1974**, *60*, 2488.
(41) Meijer, A. J. H. M.; Goldfield, E. M. *J. Chem. Phys.* **1999**, *110*, 870.
(42) Lin, S. Y.; Guo, H. *J. Phys. Chem.* **2004**, *A108*, 2141.
(43) Rackham, E. J.; Huarte-Larranaga, F.; Manolopoulos, D. E. *Chem. Phys. Lett.* **2001**, *343*, 356.
(44) Rackham, E. J.; Gonzalez-Lezana, T.; Manolopoulos, D. E. *J. Chem. Phys.* **2003**, *119*, 12895.
(45) Alexander, M. H.; Rackham, E. J.; Manolopoulos, D. E. *J. Chem. Phys.* **2004**, *121*, 5221.
(46) Lin, S. Y.; Guo, H. *J. Chem. Phys.* **2004**, *120*, 9907.
(47) Lin, S. Y.; Guo, H. *J. Phys. Chem.* **2004**, *A108*, 10060.
(48) Lin, S. Y.; Guo, H. *J. Chem. Phys.* **2005**, *122*, 074304.
(49) Lin, S. Y.; Rackham, E. J.; Guo, H. *J. Phys. Chem.*, in press.
(50) Light, J. C. *J. Chem. Phys.* **1964**, *40*, 3221.
(51) Pechukas, P.; Light, J. C. *J. Chem. Phys.* **1965**, *42*, 3281.
(52) Pechukas, P.; Light, J. C.; Rankin, C. *J. Chem. Phys.* **1966**, *44*, 794.
(53) Miller, W. H. *J. Chem. Phys.* **1970**, *52*, 543.
(54) Chen, R.; Guo, H. *Comput. Phys. Commun.* **1999**, *119*, 19.
(55) Kosloff, D.; Kosloff, R. *J. Comput. Phys.* **1983**, *52*, 35.
(56) Echave, J.; Clary, D. C. *Chem. Phys. Lett.* **1992**, *190*, 225.
(57) Wei, H.; Carrington, T., Jr. *J. Chem. Phys.* **1992**, *97*, 3029.
(58) Light, J. C.; Carrington, T., Jr. *Adv. Chem. Phys.* **2000**, *114*, 263.
(59) Quack, M.; Troe, J. *Ber. Bunsen-Ges. Phys. Chem.* **1974**, *78*, 240.